

Optically addressing single rare-earth ions in a nanophotonic cavity

Tian Zhong,^{1,2,3} Jonathan M. Kindem,^{2,3} John G. Bartholomew,^{2,3} Jake Rochman,^{2,3} Ioana Craiciu,^{2,3} Varun Verma,⁴ Sae Woo Nam,⁴ Francesco Marsili,⁵ Matthew D. Shaw,⁵ Andrew D. Beyer,⁵ and Andrei Faraon^{2,3,*}

¹*Institute of Molecular Engineering, University of Chicago, Chicago, IL 60637, USA*

²*Kavli Nanoscience Institute and Thomas J. Watson, Sr., Laboratory of Applied Physics, California Institute of Technology, Pasadena, California 91125, USA.*

³*Institute for Quantum Information and Matter, California Institute of Technology, Pasadena, California 91125, USA.*

⁴*National Institute of Standards and Technology,*

325 Broadway, MC 815.04, Boulder, Colorado 80305, USA

⁵*Jet Propulsion Laboratory, California Institute of Technology, 4800 Oak Grove Drive, Pasadena, California 91109, USA*

(Dated: March 21, 2018)

Detection and control of single rare-earth dopants in solids is an important step towards quantum devices that take full advantage of the outstanding coherence properties of rare-earth ions in both optical and spin degrees of freedom. Coupling the 4f-4f transitions of ions to photonic resonators with highly confined optical modes provides an effective approach to overcome their weak photoluminescence emission and poor photon collection efficiency, which have so far hindered the experimental progress on optical isolation and control of single rare-earth emitters. Here we demonstrate a nanophotonic platform based on a yttrium orthovanadate (YVO) photonic crystal nanobeam resonator coupled to spectrally resolved individual neodymium (Nd^{3+}) ions. The strong emission enhancement in the nanocavity enables optical addressing of single Nd^{3+} ions. The ions show near-radiatively-limited single photon emissions. The measured high coupling strength between a single photon and the ion allows for optical Rabi oscillations and a high coupling cooperativity, which could enable optically controlled spin qubits, quantum logic gates, and spin-photon interfaces in future quantum networks.

Rare-earth dopants in solids exhibit long-lived coherence in both optical and spin degrees of freedom [1, 1]. The effective shielding of their 4f electrons leads to optical and radio-frequency transitions with less sensitivity to electronic and magnetic noise in their crystalline surroundings at cryogenic temperatures. Significant progress in rare-earth based quantum technologies has led to ensemble-based optical quantum memories [3–6] and coherent transducers [7], with promising performance as efficient quantum light-matter interfaces for quantum networks. On the other hand, addressing single ions has remained an outstanding challenge, with the progress hindered by long optical lifetimes of rare-earth ions and resultant faint photoluminescence (PL). So far, only a few experiments have succeeded in isolating individual praseodymium [8–10], Cerium [11–13], and erbium [14, 15] ions, though majority of them were not probing ions via their highly coherent 4f-4f optical transitions. Recently, several works have demonstrated significant enhancement of spontaneous emissions of rare-earth emitters coupled to a nanophotonic cavity [6, 15–17], among which [6, 16] also showed little detrimental effect on the coherence properties of ions in nanodevices. These results point at a viable approach to efficiently detect and coherently control individual ions in a chip-scale architecture.

Here we demonstrate a nanophotonic platform based on a yttrium orthovanadate (YVO) photonic crystal nanobeam resonator coupled to spectrally resolved in-

dividual neodymium (Nd) ions. While the system acts as an ensemble quantum memory when operating at the center of the inhomogeneous line [6], it also enables direct optical addressing of single Nd^{3+} in the tails of the inhomogeneous distribution, which show strongly enhanced, near-radiatively-limited single photon emissions. A measured vacuum Rabi frequency of $2\pi \times 28.5$ MHz significantly exceeds the linewidth of a Nd^{3+} ion, potentially allowing coherent manipulation of single spins with optical pulses. Unlike prior experiments [8–13], this technique does not hinge on spectroscopic details of a specific type of ion and can be readily extended to other rare-earths or defect centers. It opens up new opportunities of spectroscopy on single ions that are distinct from conventional ensemble measurements, which offers a probe for local nanoscopic environment around individual rare-earth ions and may lead to new quantum information processing, interconnect and sensing devices.

Our experiment builds upon a triangular nanobeam photonic crystal resonator [16, 18] that was fabricated in a nominally 50 parts per million (ppm) doped Nd:YVO crystal using focused ion beam (FIB) milling [18]. The device is a one-sided cavity, as the input (left mirror in Fig.1(a,b)) has a lower reflectivity. The optical coupling in/out of the device was implemented via a 45° -angled coupler [16]. An aspheric doublet matches the mode of the single mode fiber to that of the nanobeam waveguide (Fig.1(a)). The coupling efficiency was optimized to 19% (from fiber to waveguide) using a 3-axis nano-positioner.

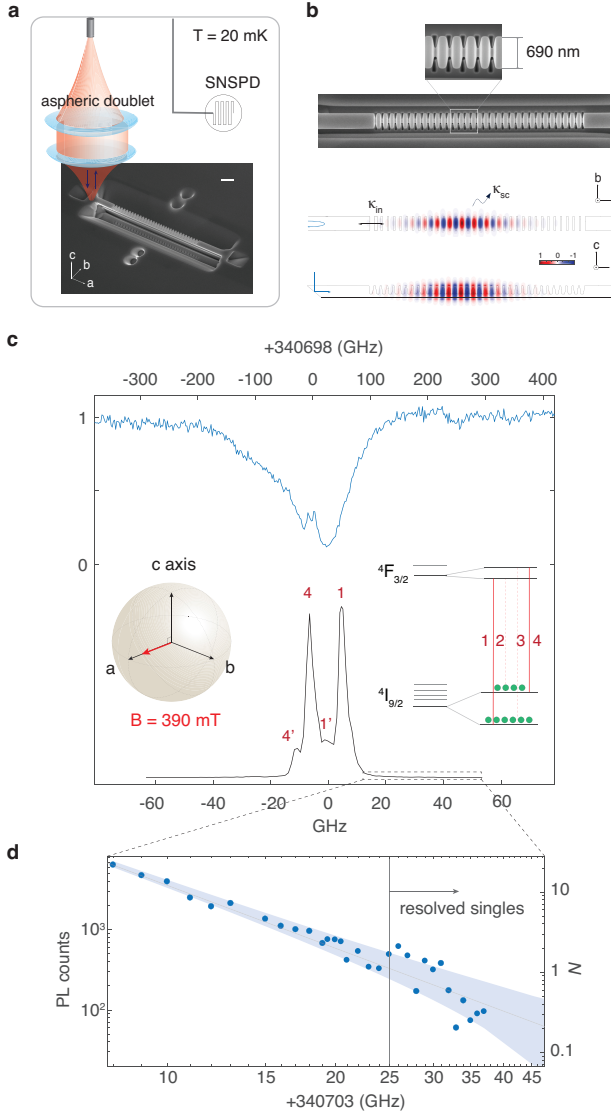


FIG. 1: (a) Schematics of the experiment in a dilution refrigerator. Scale bar is $1\mu\text{m}$. (b) SEM images of the one-sided nanobeam photonic crystal cavity in YVO fabricated using FIB. Lower panel shows simulated the TM fundamental mode profile, which has the polarization aligned to dipoles of Nd^{3+} along the crystallographic c axis. (c) Cavity reflection spectrum (upper) and Nd^{3+} photoluminescence (PL) spectrum (lower). Insets show the applied magnetic field and resulting Zeeman levels and transitions. PL from ions in the bulk substrate ($1'$ and $4'$) appear red-shifted from ions coupled to the cavity (1 and 4). (d) Atomic spectra density versus detuning on the shorter wavelength tail of the inhomogeneous distribution. The shaded area shows the projected atomic shot noise.

The nanocavity fundamental mode volume is $V_{\text{mode}} = 0.056 \mu\text{m}^3$ (simulated) with a measured quality factor $Q = 3,900$ (energy decay rate $\kappa = 2\pi \times 90 \text{ GHz}$). The waveguide-cavity coupling κ_{in} through the input mirror was 45% of κ . The device was cooled to $\sim 20 \text{ mK}$ base temperature in a dilution refrigerator, though the device

effective temperature was estimated to be around 500 mK (by comparing the ground Zeeman level populations from the PL spectra). The elevated temperature was attributed to the diminishing thermal conductance in the nanobeam. The laser for probing the ions was modulated by two double-pass acousto-optic (AOM) modulators, and delivered to the sample via a single-mode fiber. The reflected signal from the device was sent via a circulator to a superconducting nanowire single photon detector (SNSPD) that measured a 82% detection efficiency at 880 nm and $< 2 \text{ Hz}$ dark counts [6]. The SNSPD was mounted in the same fridge at the 100 mK stage. The overall photon detection efficiency including transmission to the cavity to the detector and the detection efficiency was 3.6% (Supplementary material [19]).

A typical cavity reflection spectrum when it was tuned nearly on resonance with the $\text{Nd } ^4F_{3/2}(Y_1) - ^4I_{9/2}(Z_1)$ transition at 880 nm is shown in Fig.1(c). A 390 mT magnetic field was applied along the crystallographic a axis of YVO, giving rise to split Zeeman levels and four possible optical transitions [3] (labelled 1-4) shown in the inset. Symmetry considerations impose that the 2, 3 cross transitions are forbidden, and the 1, 4 transitions are close to cyclic [4, 6]. The PL emission spectrum (with a 200-ns pulsed resonant laser excitation) is shown in the lower part of Fig.1(c). Two weak lines labelled $1'$ and $4'$ were identified as emissions from Nd ions in the bulk substrate, which are red-detuned from ions coupled to the cavity by 2.5 GHz . This shift is due to a static strain in the nanobeam, which makes it easier to spectrally separate the ions in the cavity from the bulk. For subsequent experiments, we focus on the shorter wavelength tail of the inhomogeneous distribution. Figure 1(d) plots the resonant PL against frequency detuning from the peak of line 1 (340703.0 GHz). The PL and thus the atomic spectral density (N ions per excitation pulse bandwidth) fits with a power law of $N \propto \Delta^{-2.9}$, where Δ is the detuning from the center of line 1. The 2.9 power exponent corresponds to a strain-induced broadening according to [22]. Statistical fine structures (SFS) [23] were also evident. By fitting the SFS with the projected shot noise of N (i.e. \sqrt{N} indicated as the shaded area), it is projected that discrete single ion spectra ($N < 1$) emerge at a detuning $> 25 \text{ GHz}$.

To search for spectrally resolved single ions, we scanned the center frequency of a 200-ns resonant excitation pulse around $\sim 30 \text{ GHz}$ blue detuning from the peak of line 1, and measured the PL integrated over $5 \mu\text{s}$ after the excitation. The repetition rate of the excitation pulses was 25 kHz , and the integration time was 20 seconds at each frequency. The laser was frequency stabilized to a vacuum cell reference cavity attaining a narrowed linewidth of $< 5 \text{ kHz}$ and a long term drift $< 100 \text{ kHz/day}$. Figure 2(a) shows the measured PL over a few GHz range. A handful of peaks, such as the one with close-up shown in Fig.2(c), were possible sin-

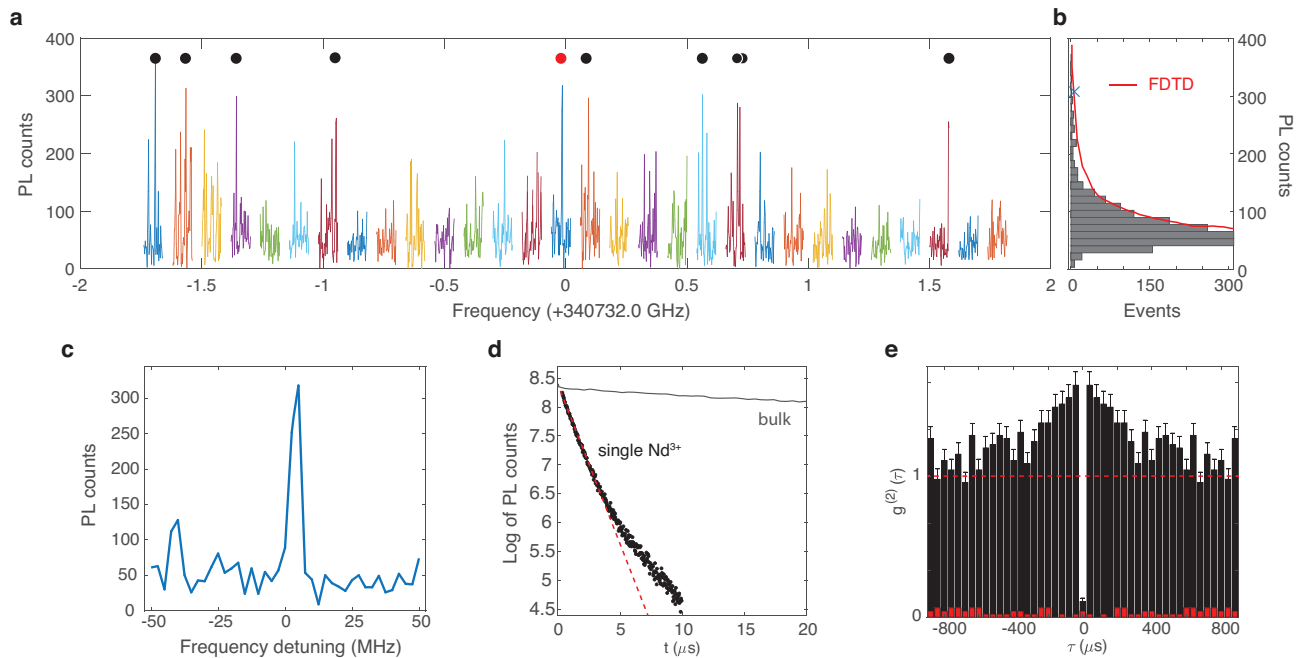


FIG. 2: (a) Photoluminescence (PL) spectrum using a 200-ns excitation pulse swept over 3 GHz around $\Delta \sim 30$ GHz. Isolated peaks marked by filled circles correspond to coupled individual Nd ions. (b) Histogram of PL intensities for an ensemble of Nd^{3+} . The red curve is a FDTD simulation of the expected distribution of the PL intensity given the different position of each ion inside the cavity. (c) PL spectrum around the ion labelled with the red circle in Fig.2(a). (d) PL decay of the isolated ion (black) with a fitted $T_1 = 2.1 \pm 0.2 \mu\text{s}$ (red dotted line), corresponding to a Purcell enhancement factor of ~ 156 compared to bulk (grey). (e) Intensity autocorrelation measurement on the single Nd^{3+} in (c) showing strong anti-bunching ($g^{(2)}(0) = 0.09 \pm 0.013$). The background signal with an off-resonant excitation is plotted in red.

gle Nd^{3+} ions. The PL intensities were histogrammed in Fig.2(b) to reveal a distribution of ion-cavity coupling strengths, which is in good agreement with that from the finite difference time domain (FDTD) simulation as plotted in red. Thus, the PL intensity serves to correlate the coupling strength of each ion with its spatial position relative to the cavity anti-nodes: an ion located exactly at the antinode with the highest field intensity would have the strongest coupling and show the highest PL. The linewidth of the peak in Fig.2(c) was broadened by the Rabi frequency of the excitation pulse. The actual linewidth of single ions was expected to be considerably narrower. With the laser tuned on-resonance with one of the peak (marked with a red dot in Fig.2(a)), the intensity autocorrelation measurement using a single detector yielded a $g^{(2)}(0) = 0.09 \pm 0.013$ (Fig.2(e)), which was normalized to $g^{(2)}(t)$ at large t . The bunching behavior at $|t| < 400 \mu\text{s}$ was expected from a multilevel emitter. The imperfect anti-bunching was partly due to a continuum of ions that is weakly coupled to the cavity, resulting in a background as in red in Fig.2(e). This background was measured with the excitation laser far detuned from the single ion resonance. The optical T_1 of this ion was $2.1 \pm 0.2 \mu\text{s}$ (Fig. 2(d)), which is strongly enhanced compared to the bulk T_1 of $90 \mu\text{s}$. The lifetime enhancement corresponded to a Purcell factor of 156 of

the probed Y_1 - Z_1 transition rate considering a branching ratio of $\beta = 0.273$ (the ground state splits into five Kramers doublets Z_1 - Z_5) [4]. The theoretically maximum Purcell factor was $F \approx \frac{3}{4\pi^2\chi_L} \left(\frac{\lambda}{n}\right)^3 \frac{Q}{V} = 189$ [24, 25] assuming a perfect alignment of the dipole with the cavity mode and $\chi_L = (3n^2/(2n^2 + 1))^2$ is the local correction to the electric field since the ion is less polarizable than the bulk medium [26]. The discrepancy is attributed to the non-optimal position of the ion with respect to the cavity anti-node, and the actual mode volume of the cavity being different from simulation because of fabrication imperfections.

The small mode volume of the nanocavity results in a significant enhancement of the coupling strength or the vacuum Rabi frequency g_0 . Focusing on the same ion in Fig.2(c), Fig.3(a) plots the PL excited by a square 250-ns resonant excitation pulse with increasing cavity mean photon number \bar{n} . The value of \bar{n} was calculated from the input pulse energy, all losses in the setup up to the device, and coupling rates of the photonic crystal mirrors (Supplementary Material [19]). The PL shows Rabi oscillations similar to an optical nutation signal [27]. The inset plots the extracted Rabi frequencies Ω versus square root of \bar{n} from the peaks (corresponding to odd integer of π pulse areas) and valleys (even integer of π pulses) of the Rabi oscillations. The slope corresponds to $g_0 = \Omega/2\sqrt{\bar{n}}$

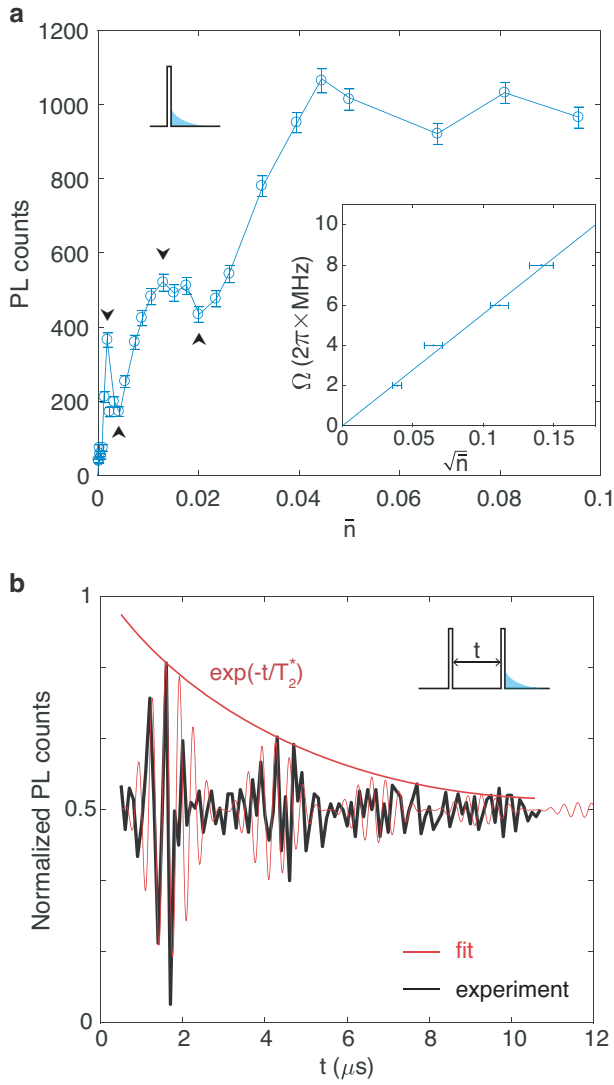


FIG. 3: (a) Rabi oscillations of PL following a pulsed resonant excitation with increasing photon number \bar{n} . Black arrows point to pulse areas that are integer multiples of π . The inset plots extracted Rabi frequencies against $\sqrt{\bar{n}}$ with a linear fit. (b) Normalized Ramsey interference fringes by subtracting a T_1 decay background from the raw PL. The beating corresponds to a 740 kHz superhyperfine coupling between Nd and Y spins.

$= 2\pi \times 28.5$ MHz, which is in agreement with the theoretical estimation of $g_0 = \mu/n\sqrt{\omega_0/2\hbar\epsilon_0V} = 2\pi \times 28.0$ MHz [24], where $\mu = 8.5 \times 10^{-32}$ C·m is the transition dipole moment (calculated using an oscillator strength $f = 8 \times 10^{-6}$ [1]), $n = 2.1785$ is the refractive index of YVO, ω_0 is the transition frequency, and ϵ_0 is the vacuum permittivity. This g_0 value is orders of magnitude stronger than the linewidth of the emitter, which makes possible the use of hard optical pulses [28] to coherently control the single ion. Next, we applied two $\pi/2$ pulses to measure the Ramsey interference of the Nd^{3+} as shown in Fig.3(b). The normalized Ramsey fringes (subtracting

a T_1 decay background) reveal a clear beating, which we believe corresponds to the superhyperfine interactions between Nd spins with the nuclear spins of yttrium in YVO. The measured superhyperfine splitting, confirmed by the two-pulse photon echo measurement (Supplementary materials), was 740 kHz, which is consistent with the ~ 2 MHz/T observed in [2]. The decay of the Ramsey fringe envelope can be fitted (red curve in Fig. 3(b)) to extract a $T_2^* = 4.0 \pm 0.2 \mu\text{s}$. From that, the spectral indistinguishability is calculated as $T_2/(2T_1) = 0.952$, indicating that the linewidth of this ion approaches the radiatively-limited regime.

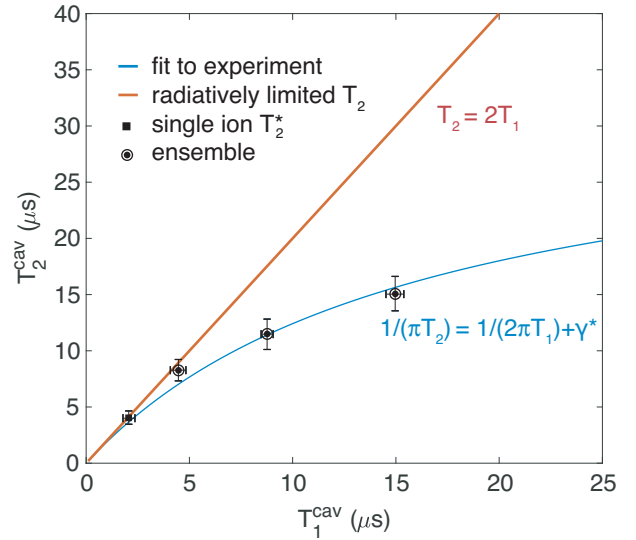


FIG. 4: Measured and theoretical optical coherence times for Nd^{3+} coupled to the cavity with varying detuning and Purcell enhancement. The red line is the radiatively-limited T_2 time. The single Nd^{3+} on resonance with the cavity (square) exhibits a near radiatively-limited linewidth with a spectral indistinguishability $> 95\%$.

The use of single rare-earth ions as spin-photon interfaces to entangle remote quantum nodes requires each emitter's linewidth to be radiatively limited. To further characterize the coherence of the ions coupled to the cavity, we performed additional ensemble two-photon echo measurements when the emitters have different detunings from cavity resonance. The ensemble T_2 times are plotted against optical T_1 decay times in Fig.4, including the single ion T_2^* data as denoted by the square. The experimental data were fitted with the relationship $1/(\pi T_2) = 1/(2\pi T_1) + \gamma^*$, where γ^* is the pure dephasing rate of the emitters. The fit (blue curve) gives a $\gamma^* = 9.7 \pm 0.6$ kHz. While slow, this dephasing rate was attributed to the superhyperfine interactions since it closely matches the superhyperfine-limited T_2 in Nd:YVO [1]. The contribution from Nd spin flip-flops are expected to be small, because the measured T_2 in a nominally undoped YVO crystal (residue doping estimated at 0.2

parts per million) was comparable to that measured in the current device (Supplementary material [19]).

The full radiatively limited $T_2=2T_1$ is plotted in red. With weak Purcell enhancement when the ions are detuned from the cavity resonance, the Nd^{3+} ions exhibit poor indistinguishabilities as indicated by the sizeable gap between the red and blue curves. Only when the ions are coupled to the cavity resonantly, do the emitters become radiatively limited. A similar approach has been used to improve the single photon indistinguishabilities of quantum dots [30]. To increase the indistinguishability, improving the cavity quality factor to further reduce T_1 would be a straightforward step, which would also allow the device to operate at higher temperatures with stronger dephasing while still achieving radiatively limited emissions. The current linewidth of the single emitter was based on T_2^* values measured over a few μs time scale (Fig.3(b)). For longer time scales (100 μs to ms), as required in quantum memories for long-distance quantum network, the slow spectral diffusion of the emitter needs to be investigated. In general, rare-earth emitters in hosts with weaker nuclear spin baths such as yttrium orthosilicate and yttrium oxide are less susceptible to spectral diffusion. Furthermore, non-Kramers ions do not have superhyperfine couplings with the host spin baths, and may offer some advantages in terms of long term narrow linewidths.

In conclusion, we have optically detected single Nd^{3+} ions coupled to a nanophotonic cavity, which enhanced the emitter spontaneous emission rate to the extent that the linewidth of the emitter became close to radiatively-limited. Optical Rabi oscillations of the single Nd^{3+} yielded a vacuum Rabi frequency $g_0=2\pi\times 28.5$ MHz, and a linewidth of 12.5 kHz ($\gamma_h=1/(\pi T_2)$, where $T_2=25.4$ μs is the emitter homogeneous linewidth without cavity enhancement (Supplementary material [19])). Given the cavity decay of $\kappa=2\pi\times 90$ GHz, the single ion cooperativity is $4g_0^2/\kappa\gamma_h=2.9$. This value could be improved significantly by using cavities with higher Q ($\times 10$ higher Q devices already demonstrated in [18] would attain an indistinguishability $>99.5\%$ and $C\sim 30$), thus making feasible the implementation of high-fidelity non-destructive detection of optical photons with a single rare-earth ion [31]. Nevertheless, questions remain regarding the spin coherence and the qubit storage time of single ions [32], and spectral diffusion occurring at longer time scales. When two spectrally resolved ions are nearby, their dipole-dipole interaction can also be probed [33]. Single rare-earth ions could be used to probe the field and temperature of its nanoscopic surroundings. Finally, the large inhomogeneous linewidth of the emitters may facilitate spectral multiplexing of individual quantum emitters for expanded bandwidth of quantum communication networks.

This work was funded by a National Science Foundation (NSF) Faculty Early Career Development Pro-

gram (CAREER) award (1454607), the AFOSR Quantum Transduction Multidisciplinary University Research Initiative (FA9550-15-1-002), and the Defense Advanced Research Projects Agency Quiness program (W31P4Q-15-1-0012). Equipment funding was also provided by the Institute of Quantum Information and Matter, an NSF Physics Frontiers Center with support from the Moore Foundation. The device nanofabrication was performed in the Kavli Nanoscience Institute at the California Institute of Technology. Part of the research was carried out at the Jet Propulsion Laboratory, California Institute of Technology, under a contract with the National Aeronautics and Space Administration. T. Zhong would like to thank Neil Sinclair, Ruffin Evans, Alp Sipahigil for experimental assistance and technical discussions.

* Electronic address: faraon@caltech.edu

- [1] C. W. Thiel, T. Böttger, and R. L. Cone, *J. Luminesc.* **131**, 353-361(2001).
- [2] Y. Sun, C. W. Thiel, R. L. Cone, R. W. Equall, and R. L. Hutcheson, *J. Lumin.* **98**, 281-287 (2002).
- [3] W. Tittel, M. Afzelius, T. Chanelière, R. L. Cone, S. Kröll, S. A. Moiseev, M. Sellars, *Laser & Photon. Rev.* **4**, 244-267 (2010).
- [4] H. de Riedmatten, M. Afzelius, M. U. Staudt, C. Simon, and N. Gisin, *Nature* **456**, 773-777 (2008).
- [5] M. P. Hedges, J. J. Longdell, Y. Li, and M. J. Sellars, *Nature* **465**, 1052-1056 (2010).
- [6] T. Zhong, *et al. Science* **357**, 1392-1395 (2016).
- [7] L. A. Williamson, Y.-H., Chen, and J. J. Longdell, *Phys. Rev. Lett.* **113**, 203601 (2014).
- [8] R. Kolesov *et al. Nat. Commun.* **3**, 1029 (2012).
- [9] T. Utikal, *et al. Nat. Commun.* **5**, 3627 (2014).
- [10] I. Nakamura, T. Yoshihiro, H. Inagawa, S. Fujiyoshi, and M. Matsushita, *Sci. Rep.* **4**, 7364 (2014).
- [11] R. Kolesov, *et al. Phys. Rev. Lett.* **111**, 120502 (2013).
- [12] P. Siyushev, *et al. Nat. Commun.* **5**, 3895 (2014).
- [13] K. Xia, *et al. Phys. Rev. Lett.* **115**, 93602 (2015).
- [14] C. Yin, M. Rancic, G. G. de Boo, N. Stavrias, J. C. McCallum, M. J. Sellars, and S. Rogge, *Nature* **497**, 91-95 (2013).
- [15] A. Dibos, M. Raha, C. Phenicie, and J. Thompson, arXiv: 1711.10368 (2017).
- [16] T. Zhong, J. M. Kindem, E. Miyazono, and A. Faraon, *Nat. Commun.* **6**, 8206 (2015).
- [17] T. Zhong, J. M. Kindem, J. Rochman, and A. Faraon, *Nat. Commun.* **8**, 14107 (2017).
- [18] T. Zhong, J. Rochman, J. M. Kindem, E. Miyazono, and A. Faraon, *Opt. Express* **24**, 536-544 (2016).
- [19] Supplementary materials.
- [20] S. R. Hasting-Simon, *et al. Phys. Rev. B* **77**, 125111 (2008).
- [21] M. Afzelius, *et al. J. Luminescence* **130**, 1566-1571 (2010).
- [22] A. M. Stoneham, *Rev. Mod. Phys.* **41**, 82-108 (1969).
- [23] W. E. Moerner and T. P. Carter, *Phys. Rev. Lett.* **59**, 2705 (1987).
- [24] D. L. McAuslan and J. J. Longdell, *Phys. Rev. A* **80**,

- 062307 (2009).
- [25] E. M. Purcell, *Phys. Rev.* **69**, 681 (1946).
 - [26] H. T. Dung, S. Y. Buhmann, and D.-G. Welsch, *Phys. Rev. A* **74**, 023803 (2006).
 - [27] I. Gerhardt, G. Wrigge, G. Zumofen, J. Hwang, A. Renn, and V. Sandoghdar, *Phys. Rev. A* **79**, 011402(R) (2009).
 - [28] G. J. Pryde, M. J. Sellars, and N. B. Manson, *Phys. Rev. Lett.* **84**, 1152-1155 (2000).
 - [29] I. Usmani, M. Afzelius, H. de Riedmatten, and N. Gisin, *Nature Commun.* **1**, 12 (2010).
 - [30] T. Grange, *et al.* *Phys. Rev. Lett.* **118**, 253602 (2017).
 - [31] C. O' Brien, T. Zhong, A. Faraon, C. Simon, *Phys. Rev. A* **94**, 043807 (2016).
 - [32] G. Wolfowicz, *et al.* *Phys. Rev. Lett.* **114**, 170503 (2015).
 - [33] J. J. Longdell and M. J. Sellars, *Phys. Rev. A* **69**, 032307 (2004).

SUPPLEMENTARY MATERIAL FOR OPTICALLY ADDRESSING SINGLE RARE-EARTH IONS IN A NANOPHOTONIC CAVITY

More details on the experimental setup

Figure S1 illustrates the experimental setup with more details. The Nd:YVO sample crystal was soldered with indium onto a copper plate that was mounted on top of a 3-axis nanopositioner, and was thermally connected to the 20 mK base plate of the dilution refrigerator. Cavity tuning was realized by gas condensation using N₂ gas. The gas tube (brown line in Fig. S1) was thermally anchored to the 3.8 K stage. When performing gas tuning, a heater on the gas tube heats it up to >30 K to allow gas to flow through. The heater was turned off after tuning. This configuration was to minimize the heat load generated by the tube, allowing the lowest possible temperature at the sample.

Fiber-waveguide coupling efficiency The fiber-waveguide coupling efficiency was characterized by measuring the reflection of a pulse far off resonance with the cavity (i.e. in the photonic bandgap). The pulse propagated from point 1 (marked in Fig.S1) to 2, 3, and was reflected back to 2, then 4. The transmission efficiency from 1 to 2 (64.1%), and from 2-4 (51.7%) were directly measured. The only unknown was the coupling efficiency from 2 to 3. Therefore, this coupling efficiency could be uniquely determined from the total pulse reflection, and was measured to be 19%.

Photon collection efficiency For each photon emitted by an ion into the cavity, the probability of that photon transmitted to the coupling waveguide was $\kappa_{in}/\kappa=45\%$. The photon then propagated from 3 to 2 (19% waveguide-fiber coupling), and from 2 to 4 (79.9% transmission through all fiber slices/connectors and 64.7% transmission through the optical circulator), and was finally detected by the 82%-efficient superconducting nanowire detector. Thus the overall collection efficiency for a cavity photon was $0.45 \times 0.19 \times 0.80 \times 0.65 \times 0.82 = 3.6\%$.

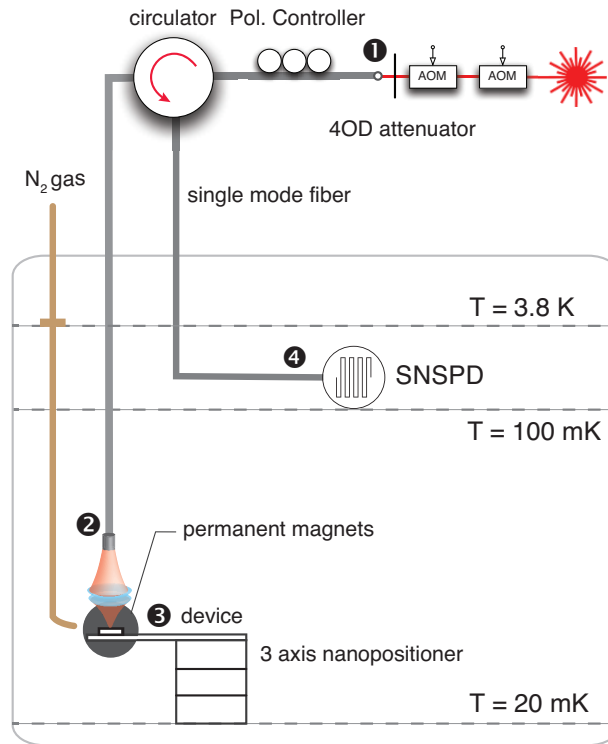


FIG. S1: Details of the experimental setup. SNSPD: superconducting nanowire single photon detector.

Cavity mean photon number To obtain the cavity mean photon number in Fig.3, we first calculate the peak power of the excitation pulse in the waveguide i.e. P_{in} with the knowledge of transmission from 1 to 2 and the coupling efficiency from 2 to 3. The cavity mean photon number was $\bar{n} = 4P_{in}\kappa_{in}/\hbar\omega_0\kappa^2$, where $\kappa_{in} = 2\pi \times 40$ GHz was the cavity in-coupling rate, $\kappa = 2\pi \times 90$ GHz was the total cavity decay rate, and ω_0 is the photon frequency.

Photon echo measurements

Two pulse photon echo measurements were performed on an ensemble of ions in the cavity near the center of inhomogeneous distribution (e.g. line 1). The cavity resonance was tuned to different frequencies using gas condensation technique to obtain homogeneous linewidths of ions at varying Purcell enhancement conditions. Fig.S2 plots photon echo decays at ensemble-cavity detuning of $\delta \sim 22$ and ~ 50 GHz. Oscillations in the echo intensities correspond to superhyperfine interactions between Nd spins and Y nuclear spins [2] at 740 kHz, which agree with the beat frequency observed in the Ramsey interference fringes. Note that the period of the oscillations appear to be twice long in the Ramsey fringes than the echo decays, because the photon echo is emitted after twice the delay between two pulses. The T_2 were fitted from the linear section of the decay, which started after approximately 4 μs .

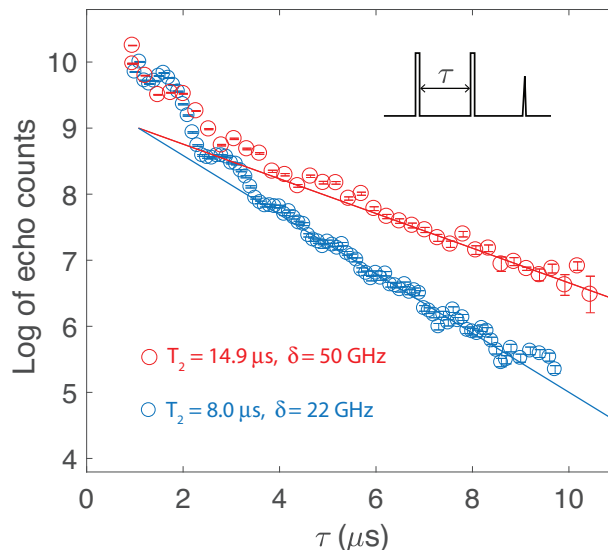


FIG. S2: Photon echoes on sub-ensembles of Nd ions coupled to the cavity at different cavity-ensemble detunings. Oscillations evident in the initial echo intensity decays were due to superhyperfine couplings between Nd and Y spins. T_2 was fitted from the linear decay sections ($>4 \mu\text{s}$). A difference in T_2 at varying detunings reflects the change of radiative decay rates (i.e. T_1) under different Purcell enhancement factors.

OPTICAL DEPHASING IN Nd:YVO

Possible contributions to the optical dephasing $\gamma^* = 9.7$ kHz include superhyperfine coupling between Nd spins and yttrium/vanadium nuclear spins, the Nd spin flip-flops, direct phonon couplings, and other higher order processes. Here we discuss contributions from two potentially dominant mechanisms.

Superhyperfine interaction The experimental condition in the current work closely reassembles that in [1] in which optical T_2 for a 10 ppm doped Nd:YVO sample was measured at varying magnetic field applied along the a-axis of the crystal. It was found in [1] that with a field greater than 1.5 T, the T_2 of 27 μs became limited by the superhyperfine interaction. The corresponding dephasing rate could be calculated from $1/(\pi/T_2) - 1/(\pi/2T_1) = 10.0$ kHz, which was very close to the currently measured dephasing. We thus expect that the superhyperfine interactions contribute substantially to the measured γ^* .

Nd spin flip-flops Dephasing due to the Nd spin flip-flops is a function of the Nd doping concentration and temperature. To better understand this process, we measured optical T_2 times in both the 50 ppm doped (the same crystal on which the devices were fabricated) and a nominally undoped YVO crystal. From the absorption spectroscopy and secondary ion mass spectroscopy (SIMS), we estimated the doping concentration of Nd to be ≈ 0.2 ppm in the undoped YVO. Therefore, the dephasing owing to spin flip-flops are expected to be relatively small in that sample. Both crystals were soldered to a common sample holder. With the same magnetic field configuration as in the main text, the ground level splitting was $\mu_B g_{\perp} \mathbf{B} = 12.88$ GHz where $g_{\perp} = 2.36$ is the ground state g-factor [3, 4], and $\mathbf{B} = 0.39$ T. We then used the ratio between the absorptions of two Zeeman transitions to calibrate the crystal temperature. When both crystals were at ~ 500 mK, we measured a $T_2^{\text{doped}} = 25.4 \mu\text{s}$ and $T_2^{\text{undoped}} = 27.0 \mu\text{s}$ in 50 ppm doped

and undoped YVO crystals, respectively. The difference in linewidths, which amounts to <1 kHz, serves as an upper bound on dephasing due to Nd spin flip-flops at 500 mK.

* Electronic address: faraon@caltech.edu

- [1] Y. Sun, C. W. Thiel, R. L. Cone, R. W. Equall, and R. L. Hutcheson, *J. Lumin.* **98**, 281-287 (2002).
- [2] I. Usmani, M. Afzelius, H. de Riedmatten, and N. Gisin, *Nature Commun.* **1**, 12 (2010).
- [3] S. R. Hasting-Simon, *et al. Phys. Rev. B* **77**, 125111 (2008).
- [4] M. Afzelius, *et al. J. Luminescence* **130**, 1566-1571 (2010).